7.4. Correction of systematic errors

By N. G. Alexandropoulos, M. J. Cooper, P. Suortti and B. T. M. Willis

7.4.1. Absorption

The positions and intensities of X-ray diffraction maxima are affected by absorption, the magnitude of the effect depending on the size and shape of the specimen. Positional effects are treated as they are encountered in the chapters on experimental techniques.

In structure determination, the effect of absorption on intensity may sometimes be negligible, if the crystal is small enough and the radiation penetrating enough. In general, however, this is not the case, and corrections must be applied. They are simplest if the crystal is of a regular geometric shape, produced either through natural growth or through grinding or cutting. Expressions for reflection from and transmission through a flat plate are given in Table 6.3.3.1, for reflection from cylinders in Table 6.3.3.2, and for reflection from spheres in Table 6.3.3.3. The calculation for a crystal bounded by arbitrary plane faces is treated in Subsection 6.3.3.3.

The values of mass absorption (attenuation) coefficients required for the calculation of corrections are given as a function of the element and of the radiation in Table 4.2.4.3.

7.4.2. Thermal diffuse scattering (By B. T. M. Willis)

7.4.2.1. *Glossary of symbols*

$\hat{e}_j$	Direction cosines of $\mathbf{e}_j(\mathbf{q})$
$\mathbf{e}_j(\mathbf{q})$	Polarization vector of normal mode $(j\mathbf{q})$
$E_j(\mathbf{q})$	Energy of mode $(j\mathbf{q})$
$E_{\rm meas}$	Total integrated intensity measured under Bragg peak
E_0	Integrated intensity from Bragg scattering
E_1	Integrated intensity from one-phonon scattering
$F(\mathbf{h})$	Structure factor
$\hbar$	Planck's constant h divided by 2π
$2\pi\mathbf{h}$	Reciprocal-lattice vector
$\mathbf{H}$	Scattering vector
j	Label for branch of dispersion relation
$\mathbf{k}_0$	Wavevector of incident radiation
$\mathbf{k}$	Wavevector of scattered radiation
k_B	Boltzmann's constant
m_n	Neutron mass
m	Mass of unit cell
N	Number of unit cells in crystal
$\mathbf{q}$	Wavevector of normal mode of vibration
q_m	Radius of scanning sphere in reciprocal space
V	Volume of unit cell
$\mathbf{v}_j$	Elastic wave velocity for branch j
$\mathbf{v}_L$	Mean velocity of elastic waves
α	TDS correction factor
2θ	Scattering angle
θ_B	Bragg angle
$\left(\frac{d\sigma}{d\Omega}\right)^{(0)}$	Differential cross section for Bragg scattering
$\left(\frac{d\sigma}{d\Omega}\right)^{(1)}$	Differential cross section for one-phonon scattering
ρ	Density of crystal
$\omega_j(\mathbf{q})$	Frequency of normal mode $(j\mathbf{q})$

Thermal diffuse scattering (TDS) is a process in which the radiation is scattered inelastically, so that the incident X-ray photon (or neutron) exchanges one or more quanta of vibrational energy with the crystal. The vibrational quantum is known as a phonon, and the TDS can be distinguished as one-phonon (first-order), two-phonon (second-order), ... scattering according to the number of phonons exchanged.

The normal modes of vibration of a crystal are characterized as either acoustic modes, for which the frequency $\omega(\mathbf{q})$ goes to zero as the wavevector $\mathbf{q}$ approaches zero, or optic modes, for which the frequency remains finite for all values of $\mathbf{q}$ [see Section 4.1.1 of *IT* B (1992)]. The one-phonon scattering by the acoustic modes rises to a maximum at the reciprocal-lattice points and so is not entirely subtracted with the background measured on either side of the reflection. This gives rise to the 'TDS error' in estimating Bragg intensities. The remaining contributions to the TDS – the two-phonon and multphonon acoustic mode scattering and all kinds of scattering by the optic modes – are largely removed with the background.

It is not easy in an X-ray experiment to separate the elastic (Bragg) and the inelastic thermal scattering by energy analysis, as the energy difference is only a few parts per million. However, this has been achieved by Dorner, Burkel, Illini & Peisl (1987) using extremely high energy resolution. The separation is also possible using Mössbauer spectroscopy. Fig. 7.4.2.1 shows the elastic and inelastic components from the 060 reflection of $LiNbO_3$ (Krec, Steiner, Pongratz & Skalicky, 1984), measured with γ-radiation from a ^{57}Co Mössbauer source. The TDS makes a substantial contribution to the measured integrated intensity; in Fig. 7.4.2.1, it is 10% of the total intensity, but it can be much larger for higher-order reflections. On the other hand, for the extremely sharp Bragg peaks obtained with synchrotron radiation, the TDS error may be reduced to negligible proportions (Bachmann, Kohler, Schulz & Weber, 1985).

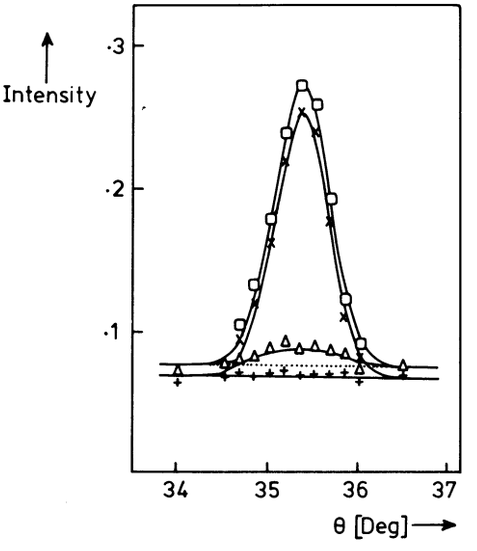

Fig. 7.4.2.1. 060 reflection of $LiNbO_3$ (Mössbauer diffraction). Inelastic (triangles), elastic (crosses), total (squares) and background (pluses) intensity (after Krec, Steiner, Pongratz & Skalicky, 1984).

Let $E_{\rm meas}$ represent the *total* integrated intensity measured in a diffraction experiment, with E_0 the contribution from Bragg scattering and E_1 that from (one-phonon) TDS. Then,

$$E_{\rm meas} = E_0 + E_1 = E_0(1+\alpha), \tag{7.4.2.1}$$

where α is the ratio E_1/E_0 and is known as the 'TDS correction factor'. α can be evaluated in terms of the properties of the crystal (elastic constants, temperature) and the experimental conditions of measurement. In the following, it is implied that the intensities are measured using a single-crystal diffractometer with incident radiation of a fixed wavelength We shall treat separately the calculation of α for X-rays and for thermal neutrons.

7.4.2.2. *TDS correction factor for X-rays (single crystals)*

The differential cross section, representing the intensity per unit solid angle for Bragg scattering, is

$$\left(\frac{{\rm d}\sigma}{{\rm d}\Omega}\right)^{(0)} = \frac{N(2\pi)^3}{V}\left|F(\mathbf{h})\right|^2\delta(\mathbf{H}-2\pi\mathbf{h}),$$

where N is the number of unit cells, each of volume V, and $F(\mathbf{h})$ is the structure factor. $\mathbf{H}$ is the scattering vector, defined by

$$\mathbf{H} = \mathbf{k} - \mathbf{k}_0,$$

with $\mathbf{k}$ and $\mathbf{k}_0$ the wavevectors of the scattered and incident beams, respectively. (The scattering is elastic, so $k = k_0 = 2\pi/\lambda$, where λ is the wavelength.) $2\pi\mathbf{h}$ is the reciprocal-lattice vector and the delta function shows that the scattered intensity is restricted to the reciprocal-lattice points.

The integrated Bragg intensity is given by

$$\begin{aligned} E_0 &= \int\int\left(\frac{{\rm d}\sigma}{{\rm d}\Omega}\right)^{(0)}{\rm d}\Omega\,{\rm d}t \\ &= N\frac{(2\pi)^3}{V}\left|F(\mathbf{h})\right|^2\int\int\delta(\mathbf{H}-2\pi\mathbf{h})\,{\rm d}\Omega\,{\rm d}t, \end{aligned} \tag{7.4.2.2}$$

where the integration is over the solid angle Ω subtended by the detector at the crystal and over the time t spent in scanning the reflection. Using

$$\int\delta(\mathbf{H})\,{\rm d}\mathbf{H} = 1,$$

with ${\rm d}\mathbf{H} = H\,{\rm d}\theta$, equation (7.4.2.2) reduces to the familiar result (James, 1962)

$$E_0 = \frac{N\lambda^3\left|F(\mathbf{h})\right|^2}{V\omega_0\sin 2\theta}, \tag{7.4.2.3}$$

where ω_0 is the angular velocity of the crystal and 2θ the scattering angle.

The differential cross section for one-phonon scattering by acoustic modes of small wavevector $\mathbf{q}$ is

$$\begin{aligned} \left(\frac{{\rm d}\sigma}{{\rm d}\Omega}\right)^{(1)} &= \frac{(2\pi)^3}{V}\left|F(\mathbf{h})\right|^2 \\ &\times\sum_{j=1}^{3}\frac{\mathbf{H}\cdot\mathbf{e}_j(\mathbf{q})}{m\omega_j^2(\mathbf{q})}E_j(\mathbf{q})\delta(\mathbf{H}\pm\mathbf{q}-2\pi\mathbf{h}) \end{aligned} \tag{7.4.2.4}$$

[see Section 4.1.1 of *IT* B (1992)]. Here, $\mathbf{e}_j(\mathbf{q})$ is the polarization vector of the mode $(j\mathbf{q})$, where j is an index for labelling the acoustic branches of the dispersion relations, m is the mass of the unit cell and $E_j(\mathbf{q})$ is the mode energy. The delta function in (7.4.2.4) shows that the scattering from the mode $(j\mathbf{q})$ is confined to the points in reciprocal space displaced by $\pm\mathbf{q}$ from the reciprocal-lattice point at $\mathbf{q}=0$. The acoustic modes involved are of small wavenumber, for which the dispersion relation can be written

$$\omega_j(\mathbf{q}) = \mathbf{v}_j\left|\mathbf{q}\right|, \tag{7.4.2.5}$$

where $\mathbf{v}_j$ is the velocity of the elastic wave with polarization vector $\mathbf{e}_j(\mathbf{q})$. Substituting (7.4.2.5) into (7.4.2.4) shows that the intensity from the acoustic modes varies as $1/q^2$, and so peaks strongly at the reciprocal-lattice points to give rise to the TDS error.

Integrating the delta function in (7.4.2.4) gives the integrated one-phonon intensity

$$\begin{aligned} E_1 &= \frac{\lambda^3}{V^2\omega_0\sin 2\theta_B}H^2\left|F(\mathbf{h})\right|^2 \\ &\times\sum_q\sum_j\frac{\left[\mathbf{H}\cdot\mathbf{e}_j(\mathbf{q})\right]^2}{\rho\omega_q^2(\mathbf{q})}E_j(\mathbf{q}), \end{aligned}$$

with ρ the crystal density. The sum over the wavevectors $\mathbf{q}$ is determined by the range of $\mathbf{q}$ encompassed in the intensity scan. The density of wavevectors is uniform in reciprocal space [see Section 4.1.1 of *IT* B (1992)], and so the sum can be replaced by an integral

$$\sum_q \rightarrow \frac{NV}{(2\pi)^3}\int{\rm d}\mathbf{q}.$$

Thus, the correction factor (E_1/E_0) is given by

$$\alpha = \frac{1}{8\pi^3}\int J(\mathbf{q})\,{\rm d}\mathbf{q}, \tag{7.4.2.6}$$

where

$$J(\mathbf{q}) = \sum_j\frac{\mathbf{H}\cdot\mathbf{e}_j(\mathbf{q})^2}{\rho\omega^2(\mathbf{q})}E_j(\mathbf{q}). \tag{7.4.2.7}$$

The integral in (7.4.2.6) is over the range of measurement, and the summation in (7.4.2.7) is over the three acoustic branches. Only long-wavelength elastic waves, with a linear dispersion relation, equation (7.4.2.5), need be considered.

7.4.2.2.1. *Evaluation of* $J(\mathbf{q})$

The frequencies $\omega_j(\mathbf{q})$ and polarization vectors $\mathbf{e}_j(\mathbf{q})$ of the elastic waves in equation (7.4.2.7) can be calculated from the classical theory of Voigt (1910) [see Wooster (1962)]. If $\widehat{e}_1$, $\widehat{e}_2$, $\widehat{e}_3$ are the direction cosines of the polarization vector with respect to orthogonal axes x, y, z, then the velocity $\mathbf{v}_j$ is determined from the elastic stiffness constants c_{ijkl} by solving the following equations of motion.

$$\begin{aligned} \widehat{e}_1\left(A_{11}-\rho v_j^2\right)+\widehat{e}_2A_{12}+\widehat{e}_3A_{13} &= 0, \\ \widehat{e}_1A_{12}+\widehat{e}_2\left(A_{22}-\rho v_j^2\right)+\widehat{e}_3A_{23} &= 0, \\ \widehat{e}_1A_{13}+\widehat{e}_2A_{23}+\widehat{e}_3\left(A_{33}-\rho v_j^2\right) &= 0. \end{aligned}$$

Here, A_{km} is the km element of a 3×3 symmetric matrix $\mathbf{A}$; if $\widehat{q}_1$, $\widehat{q}_2$, $\widehat{q}_3$ are the direction cosines of the wavevector $\mathbf{q}$ with reference to x, y, z, the km element is given in terms of the elastic stiffness constants by

$$A_{km} = \sum_{l=1}^{3}\sum_{n=1}^{3}c_{klmn}\widehat{q}_l\widehat{q}_n.$$

The four indices $klmn$ can be reduced to two, replacing 11 by 1, 22 by 2, 33 by 3, 23 and 32 by 4, 31 and 13 by 5, and 12 and 21 by 6. The elements of $\mathbf{A}$ are then given explicitly by

$$
\begin{aligned}
A_{11} &= c_{11}\hat{q}_1^2 + c_{66}\hat{q}_2^2 + c_{55}\hat{q}_3^2 + 2c_{56}\hat{q}_2\hat{q}_3 \\
&\quad + 2c_{15}\hat{q}_3\hat{q}_1 + 2c_{16}\hat{q}_1\hat{q}_2, \\
A_{22} &= c_{66}\hat{q}_1^2 + c_{22}\hat{q}_2^2 + c_{44}\hat{q}_3^2 + 2c_{24}\hat{q}_2\hat{q}_3 \\
&\quad + 2c_{46}\hat{q}_3\hat{q}_1 + 2c_{26}\hat{q}_1\hat{q}_2, \\
A_{33} &= c_{55}\hat{q}_1^2 + c_{44}\hat{q}_2^2 + c_{33}\hat{q}_3^2 + 2c_{34}\hat{q}_2\hat{q}_3 \\
&\quad + 2c_{35}\hat{q}_3\hat{q}_1 + 2c_{45}\hat{q}_1\hat{q}_2, \\
A_{12} &= c_{16}\hat{q}_1^2 + c_{26}\hat{q}_2^2 + c_{45}\hat{q}_3^2 + (c_{25} + c_{46})\hat{q}_2\hat{q}_3 \\
&\quad + (c_{14} + c_{56})\hat{q}_3\hat{q}_1 + (c_{12} + c_{66})\hat{q}_1\hat{q}_2, \\
A_{13} &= c_{15}\hat{q}_1^2 + c_{46}\hat{q}_2^2 + c_{35}\hat{q}_3^2 + (c_{36} + c_{45})\hat{q}_2\hat{q}_3 \\
&\quad + (c_{13} + c_{55})\hat{q}_3\hat{q}_1 + (c_{14} + c_{56})\hat{q}_1\hat{q}_2, \\
A_{23} &= c_{56}\hat{q}_1^2 + c_{24}\hat{q}_2^2 + c_{34}\hat{q}_3^2 + (c_{23} + c_{44})\hat{q}_2\hat{q}_3 \\
&\quad + (c_{36} + c_{45})\hat{q}_3\hat{q}_1 + (c_{25} + c_{46})\hat{q}_1\hat{q}_2.
\end{aligned}
$$

The setting up of the matrix $\mathbf{A}$ is a fundamental first step in calculating the TDS correction factor. This implies a knowledge of the elastic constants, whose number ranges from three for cubic crystals to twenty one for triclinic crystals. The measurement of elastic stiffness constants is described in Section 4.1.6 of *IT* B (1992).

For each direction of propagation $\hat{\mathbf{q}}$, there are three values of ρv_j^2 $(j = 1, 2, 3)$, given by the eigenvalues of $\mathbf{A}$. The corresponding eigenvectors of $\mathbf{A}$ are the polarization vectors $\mathbf{e}_j(\mathbf{q})$. These polarization vectors are mutually perpendicular, but are not necessarily parallel or perpendicular to the propagation direction.

The function $J(\mathbf{q})$ in equation (7.4.2.7) is related to the inverse matrix $\mathbf{A}^{-1}$ by

$$J(\mathbf{q}) = \frac{k_B T}{q^2} \sum_{m=1}^{3} \sum_{n=1}^{3} \left(\mathbf{A}^{-1}\right)_{mn} H_m H_n, \tag{7.4.2.8}$$

where H_1, H_2, H_3 are the x, y, z components of the scattering vector $\mathbf{H}$, and classical equipartition of energy is assumed [$E_j(\mathbf{q}) = k_B T$]. Thus $\mathbf{A}^{-1}$ determines the anisotropy of the TDS in reciprocal space, arising from the anisotropic elastic properties of the crystal.

Isodiffusion surfaces, giving the locus in reciprocal space for which the intensity $J(\mathbf{q})$ is constant for elastic waves of a given wavelength, were first plotted by Jahn (1942). These surfaces are not spherical even for cubic crystals (unless $c_{11} - c_{12} = c_{44}$), and their shapes vary from one reciprocal-lattice point to another.

7.4.2.2.2. *Calculation of* α

Inserting (7.4.2.8) into (7.4.2.6) gives the TDS correction factor as

$$\alpha = \sum_{m=1}^{3} \sum_{n=1}^{3} T_{mn} H_m H_n, \tag{7.4.2.9}$$

where T_{mn}, an element of a 3×3 symmetric matrix $\mathbf{T}$, is defined by

$$T_{mn} = \frac{k_B T}{8\pi^3} \int \frac{\left(\mathbf{A}^{-1}\right)_{mn}}{q^2} \, \mathrm{d}\mathbf{q}. \tag{7.4.2.10}$$

Equation (7.4.2.9) can also be written in the matrix form

$$\alpha = \mathbf{H}^T \mathbf{T} \mathbf{H}, \tag{7.4.2.11}$$

with $\mathbf{H}^T = (H_1, H_2, H_3)$ representing the transpose of $\mathbf{H}$.

The components of $\mathbf{H}$ relate to orthonormal axes, whereas it is more convenient to express them in terms of Miller indices *hkl* and the axes of the reciprocal lattice. If $\mathbf{S}$ is the 3×3 matrix that transforms the scattering vector $\mathbf{H}$ from orthonormal axes to reciprocal-lattice axes, then

$$\mathbf{H} = \mathbf{S}\mathbf{h}, \tag{7.4.2.12}$$

where $\mathbf{h}^T = (h, k, l)$. The final expression for α, from (7.4.2.11) and (7.4.2.12), is

$$\alpha = \mathbf{h}^T \mathbf{S}^T \mathbf{T} \mathbf{S} \mathbf{h}. \tag{7.4.2.13}$$

This is the basic formula for the TDS correction factor.

We have assumed that the entire one-phonon TDS under the Bragg peak contributes to the measured integrated intensity, whereas some of it is removed in the background subtraction. This portion can be calculated by taking the range of integration in (7.4.2.10) as that corresponding to the region of reciprocal space covered in the background measurement.

To evaluate $\mathbf{T}$ requires the integration of the function $\mathbf{A}^{-1}$ over the scanned region in reciprocal space (see Fig. 7.4.2.2). Both the function itself and the scanned region are anisotropic about the reciprocal-lattice point, and so the TDS correction is anisotropic too, *i.e.* it depends on the direction of the diffraction vector as well as on $\sin\theta/\lambda$.

Computer programs for calculating the anisotropic TDS correction for crystals of any symmetry have been written by Rouse & Cooper (1969), Stevens (1974), Merisalo & Kurittu (1978), Helmholdt, Braam & Vos (1983), and Sakata, Stevenson & Harada (1983). To simplify the calculation, further approximations can be made, either by removing the anisotropy associated with $\mathbf{A}^{-1}$ or that associated with the scanned region. In the first case, the element T_{mn} is expressed as

$$T_{mn} = \frac{k_B T}{8\pi^3} \left\langle \left(\mathbf{A}^{-1}\right)_{mn} \right\rangle \int \frac{1}{q^2} \, \mathrm{d}q,$$

where the angle brackets indicate the average value over all directions. In the second case,

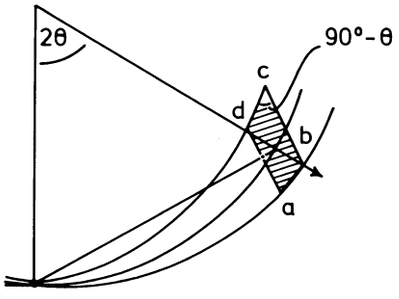

(*a*)

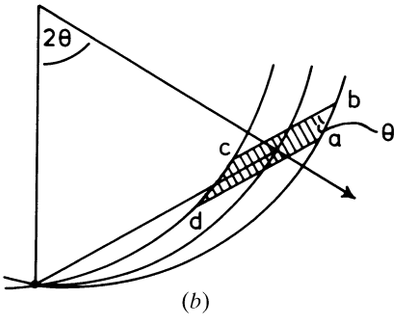

(*b*)

Fig. 7.4.2.2. Diagrams in reciprocal space illustrating the volume *abcd* swept out for (*a*) an ω scan, and (*b*) a $\theta/2\theta$, or $\omega/2\theta$, scan. The dimension of *ab* is determined by the aperture of the detector and of *bc* by the rocking angle of the crystal.

$$T_{mn} = \frac{k_B T}{8\pi^3} q_m \int\int \left(\mathbf{A}^{-1}\right)_{mn} \mathrm{d}S,$$

where q_m is the radius of the sphere that replaces the anisotropic region (Fig. 7.4.2.2) actually scanned in the experiment, and $\mathrm{d}S$ is a surface element of this sphere. q_m can be estimated by equating the volume of the sphere to the volume swept out in the scan.

If *both* approximations are employed, the correction factor is isotropic and reduces to

$$\alpha = \frac{H^2 k_B T q_m}{3\pi^2 \rho \mathbf{v}_L^2}, \qquad (7.4.2.14)$$

with $\mathbf{v}_L$ representing the mean velocity of the elastic waves, averaged over all directions of propagation and of polarization.

Experimental values of α have been measured for several crystals by γ-ray diffraction of Mössbauer radiation (Krec & Steiner, 1984). In general, there is good agreement between these values and those calculated by the numerical methods, which take into account anisotropy of the TDS. The correction factors calculated analytically from (7.4.2.14) are less satisfactory.

The principal effect of *not* correcting for TDS is to underestimate the values of the atomic displacement parameters. Writing $\exp\alpha \approx 1 + \alpha$, we see from (7.4.2.14) that the overall displacement factor is increased from B to $B + \Delta B$ when the correction is made. ΔB is given by

$$\Delta B = \frac{8 k_B T q_m}{3\pi^2 \rho \mathbf{v}_L^2}.$$

Typically, $\Delta B/B$ is 10–20%. Smaller errors occur in other parameters, but, for accurate studies of charge densities or bonding effects, a TDS correction of all integrated intensities is advisable (Helmholdt & Vos, 1977; Stevenson & Harada, 1983).

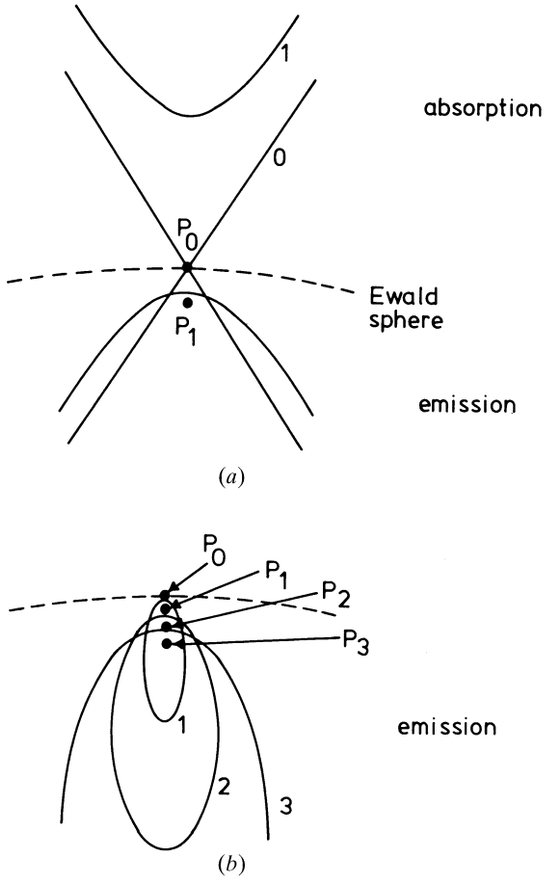

Fig. 7.4.2.3. Scattering surfaces for one-phonon scattering of neutrons: (*a*) for neutrons faster than sound ($\beta < 1$); (*b*) for neutrons slower than sound ($\beta > 1$). The scattering surface for X-rays is the Ewald sphere. P_0, P_1, *etc.* are different positions of the reciprocal-lattice point with respect to the Ewald sphere, and the scattering surfaces are numbered to correspond with the appropriate position of P.

7.4.2.3. *TDS correction factor for thermal neutrons (single crystals)*

The neutron treatment of the correction factor lies along similar lines to that for X-rays. The principal difference arises from the different topologies of the one-phonon 'scattering surfaces' for X-rays and neutrons. These surfaces represent the locus in reciprocal space of the end-points of the phonon wavevectors $\mathbf{q}$ (for fixed crystal orientation and fixed incident wavevector $\mathbf{k}_0$) when the wavevector $\mathbf{k}$ of the scattered radiation is allowed to vary. We shall not discuss the theory for pulsed neutrons, where the incident wavelength varies (see Popa & Willis, 1994).

The scattering surfaces are determined by the conservation laws for momentum transfer,

$$\mathbf{H} = \mathbf{k} - \mathbf{k}_0 = 2\pi\mathbf{h} + \mathbf{q},$$

and for energy transfer,

$$\hbar^2\left(k^2 - k_0^2\right)/2m_n = -\varepsilon\hbar\omega_j(\mathbf{q}), \qquad (7.4.2.15)$$

where m_n is the neutron mass and $\hbar\omega_j(\mathbf{q})$ is the phonon energy. ε is either $+1$ or -1, where $\varepsilon = +1$ corresponds to phonon emission (or phonon creation) in the crystal and a loss in energy of the neutrons after scattering, and $\varepsilon = -1$ corresponds to phonon absorption (or phonon annihilation) in the crystal and a gain in neutron energy. In the X-ray case, the phonon energy is negligible compared with the energy of the X-ray photon, so that (7.4.2.15) reduces to

$$k = k_0,$$

and the scattering surface is the Ewald sphere. For neutron scattering, $\hbar\omega_j(\mathbf{q})$ is comparable with the energy of a thermal neutron, and so the topology of the scattering surface is more complicated. For one-phonon scattering by long-wavelength acoustic modes with $q \ll k_0$, (7.4.2.15) reduces to

$$k = k_0 - \varepsilon\beta q,$$

where β ($= \mathbf{v}_L/\mathbf{v}_n$) is the ratio of the sound velocity in the crystal and the neutron velocity. If the Ewald sphere in the neighbourhood of a reciprocal-lattice point is replaced by its tangent plane, the scattering surface becomes a conic section with eccentricity $1/\beta$. For $\beta < 1$, the conic section is a hyperboloid of two sheets with the reciprocal-lattice point P at one focus. The phonon

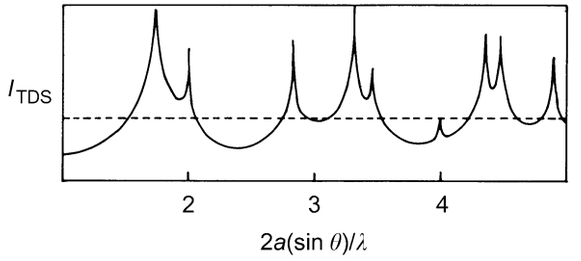

Fig. 7.4.2.4. One-phonon scattering calculated for polycrystalline nickel of lattice constant a (after Suortti, 1980).

wavevectors on one sheet correspond to scattering with phonon emission and on the other sheet to phonon absorption. For $\beta > 1$, the conic section is an ellipsoid with P at one focus. Scattering now occurs either by emission or by absorption, but not by both together (Fig. 7.4.2.3).

To evaluate the TDS correction, with **q** restricted to lie along the scattering surfaces, separate treatments are required for faster-than-sound ($\beta < 1$) and for slower-than-sound ($\beta > 1$) neutrons. The final results can be summarized as follows (Willis, 1970; Cooper, 1971):

(*a*) For faster-than-sound neutrons, the TDS rises to a maximum, just as for X-rays, and the correction factor is given by (7.4.2.13), which applies to the X-ray case. (This is a remarkable result in view of the marked difference in the one-phonon scattering surfaces for X-rays and neutrons.)

(*b*) For slower-than-sound neutrons, the correction factor depends on the velocity (wavelength) of the neutrons and is more difficult to evaluate than in (*a*). However, α will always be less than that calculated for X-rays of the same wavelength, and under certain conditions the TDS does not rise to a maximum at all so that α is then zero.

The sharp distinction between cases (*a*) and (*b*) has been confirmed experimentally using the neutron Laue technique on single-crystal silicon (Willis, Carlile & Ward, 1986).

7.4.2.4. *Correction factor for powders*

Thermal diffuse scattering in X-ray powder-diffraction patterns produces a non-uniform background that peaks sharply at the positions of the Bragg reflections, as in the single-crystal case (see Fig. 7.4.2.4). For a given value of the scattering vector, the one-phonon TDS is contributed by all those wavevectors **q** joining the reciprocal-lattice point and any point on the surface of a sphere of radius $2\sin\theta/\lambda$ with its centre at the origin of reciprocal space. These **q** vectors reach the boundary of the Brillouin zone and are not restricted to those in the neighbourhood of the reciprocal-lattice point. To calculate α properly, we require a knowledge, therefore, of the lattice dynamics of the crystal and not just its elastic properties. This is one reason why relatively little progress has been made in calculating the X-ray correction factor for powders.

7.4.3. Compton scattering
(By N. G. Alexandropoulos and M. J. Cooper)

7.4.3.1. *Introduction*

In many diffraction studies, it is necessary to correct the intensities of the Bragg peaks for a variety of inelastic scattering processes. Compton scattering is only one of the incoherent processes although the term is often used loosely to include plasmon, Raman, and resonant Raman scattering, all of which may occur in addition to the more familiar fluorescence radiation and thermal diffuse scattering. The various interactions are summarized schematically in Fig. 7.4.3.1, where the dominance of each interaction is characterized by the energy and momentum transfer and the relevant binding energy.

With the exception of thermal diffuse scattering, which is known to peak at the reciprocal-lattice points, the incoherent background varies smoothly through reciprocal space. It can be removed with a linear interpolation under the sharp Bragg peaks and without any energy analysis. On the other hand, in non-crystalline material, the elastic scattering is also diffused throughout reciprocal space; the point-by-point correction is consequently larger and without energy analysis it cannot be made empirically; it must be calculated. These calculations are imprecise except in the situations where Compton scattering is the dominant process. For this to be the case, there must be an encounter, conserving energy and momentum, between the incoming photon and an individual target electron. This in turn will occur if the energy lost by the photon, $\Delta E = E_1 - E_1$, clearly exceeds the one-electron binding energy, E_B, of the target electron. Eisenberger & Platzman (1970) have shown that this binary encounter model – alternatively known as the impulse approximation – fails as $(E_B/\Delta E)^2$.

Table 7.4.3.1. *The energy transfer, in eV, in the Compton scattering process for selected X-ray energies*

Scattering angle φ (°)	Cr $K\alpha$ 5411 eV	Cu $K\alpha$ 8040 eV	Mo $K\alpha$ 17 443 eV	Ag $K\alpha$ 22 104 eV
0	0	0	0	0
30	8	17	79	127
60	29	63	292	467
90	57	124	575	915
120	85	185	849	1344
150	105	229	1043	1648
180	112	245	1113	1757

Data calculated from equation (7.4.3.1).

The likelihood of this failure can be predicted from the Compton shift formula, which for scattering through an angle φ can be written.

$$\Delta E = E_1 - E_2 = \frac{E_1^2(1-\cos\varphi)}{mc^2[1+(E_1/mc^2)(1-\cos\varphi)]}. \qquad (7.4.3.1)$$

This energy transfer is given as a function of the scattering angle in Table 7.4.3.1 for a set of characteristic X-ray energies; it ranges from a few eV for Cr $K\alpha$ X-radiation at small angles, up to ~ 2 keV for backscattered Ag $K\alpha$ X-radiation. Clearly, in the majority of typical experiments Compton scattering will be inhibited from all but the valence electrons.

7.4.3.2. *Non-relativistic calculations of the incoherent scattering cross section*

7.4.3.2.1. *Semi-classical radiation theory*

For weak scattering, treated within the Born approximation, the incoherent scattering cross section, $(\mathrm{d}\sigma/\mathrm{d}\Omega)_{\mathrm{inc}}$, can be factorized as follows:

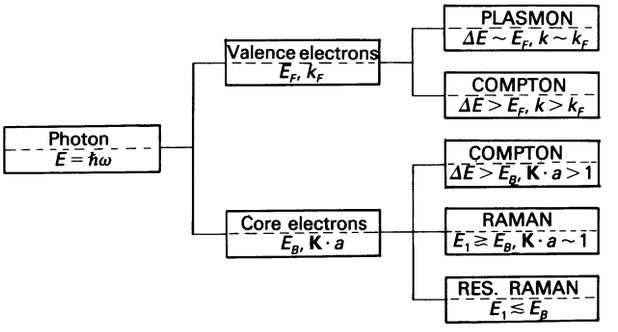

Fig. 7.4.3.1. Schematic diagram of the inelastic scattering interactions, $\Delta E = E_1 - E_2$ is the energy transferred from the photon and **K** the momentum transfer. The valence electrons are characterized by the Fermi energy, E_F, and momentum, k_F ($\hbar$ being taken as unity). The core electrons are characterized by their binding energy E_B. The dipole approximation is valid when $|\mathbf{K}|a < 1$, where a is the orbital radius of the scattering electron.

references